

PAPER

Stress spatial distributions, the Gutenberg–Richter and Omori–Utsu laws

To cite this article: François Pétrélis *et al* *J. Stat. Mech.* (2024) 043404

View the [article online](#) for updates and enhancements.

You may also like

- [Visualizing high-dimensional loss landscapes with Hessian directions](#)
Lucas Böttcher and Gregory Wheeler
- [Erratum: Exact quench dynamics of symmetry resolved entanglement in a free fermion chain \(2021 *J. Stat. Mech.* 093102\)](#)
Gilles Perez, Riccarda Bonsignori and Pasquale Calabrese
- [Precise learning curves and higher-order scaling limits for dot-product kernel regression](#)
Lechao Xiao, Hong Hu, Theodor Misiakiewicz et al.

PAPER: Interdisciplinary statistical mechanics

Stress spatial distributions, the Gutenberg–Richter and Omori–Utsu laws

François Pétrélis^{1,*}, Kristel Chanard²,
Alexandre Schubnel³ and Takahiro Hatano⁴

¹ Laboratoire de Physique de l'Ecole Normale Supérieure, ENS, Université PSL, CNRS, Sorbonne Université, Université Paris-Diderot, Paris, France

² Université de Paris, Institut de physique du globe de Paris, CNRS, IGN, F-75005 Paris, France

³ Laboratoire de Géologie, CNRS UMR 8538, Ecole Normale Supérieure, PSL Research University, Paris, France

⁴ Department of Earth and Space Science, Osaka University, 560-0043 Osaka, Japan

E-mail: petrelis@phys.ens.fr

Received 17 October 2023

Accepted for publication 18 February 2024

Published 24 April 2024



Online at stacks.iop.org/JSTAT/2024/043404

<https://doi.org/10.1088/1742-5468/ad2dd6>

Abstract. We investigate several earthquake models in one and two dimensions of space and analyze in these models the stress spatial distribution. We show that the statistical properties of stress distribution are responsible for the distribution of earthquake magnitudes, as described by the Gutenberg–Richter (GR) law. A series of predictions is made based on the analogies between the stress profile and one-dimensional random curves or two-dimensional random surfaces. These predictions include the b -value, which determines the ratio of small to large seismic events and, in two-dimensional models, we predict the existence of aftershocks and their temporal distribution, known as the Omori–Utsu law. Both the GR and Omori–Utsu law are properties which have been extensively validated by earthquake observations in nature.

Keywords: nonlinear dynamics, statistical mechanics of geophysical systems

* Author to whom any correspondence should be addressed.

Contents

1. Relation between size and moment distributions	3
2. One-dimensional models	4
2.1. Analysis of the Burridge-Knopoff (BK) model.....	4
2.2. Coulomb friction model	10
2.3. Discussion	13
3. Two-dimensional geometry	15
3.1. Description of the model	15
3.2. Numerical results.....	16
3.3. Discussion	18
3.3.1. The stress as a random surface and results from percolation theory .	18
3.3.2. The GR law and the b-value	20
3.3.3. Existence of aftershocks and the Omori–Utsu law.....	22
4. Discussion	25
4.1. Comparison with theoretical results.....	25
4.2. Comparison with natural data	27
Acknowledgments	28
References	28

Among the statistical properties of earthquakes (EQs) that were first discovered is the distribution of the energy that they release, a property that was initially described by Gutenberg and Richter [1]. Using modern definitions, the released energy during an EQ is characterized by its magnitude m defined as $m = 2\log_{10}(M)/3$ where M is the seismic moment $M = \sum \Delta x$. The sum is taken over all the spatial extent that has moved during the EQ, and Δx is the total displacement during the event. In natural seismic data, the distribution of m is observed to be an exponential, so-called Gutenberg–Richter (GR) law [1]. It is written $P(m) \propto 10^{-bm}$ and the value of b usually ranges between 3/4 and 1 [2]. When translated into the distribution of the moment M , the GR law turns into a power law distribution $P(M) \propto M^{-1-B}$, where $B = 2b/3$ and thus ranges between 1/2 and 2/3 [3].

Another well-documented property of EQs concerns the number of aftershocks, which are events that follow a large event, referred to as the mainshock. This property is called the Omori–Utsu law [4]. It is presented in general by the formula for the number n of events per unit of time $dn/dt = k/(t+c)^{-p}$ where the exponent p is of order unity, c and k are constants that depend on the mainshock properties, and t is the time elapsed since the mainshock. This is a generalization of the original formula proposed by Omori, who considered $p = 1$.

A variety of EQ models exists, using simplified and idealized dynamical rules to describe the evolution of faults [5, 6], see [3, 7] for reviews. In general, through appropriate parameter adjustment, these models yield the GR law. The objective of this article is to investigate the origin of the power-law distribution in several models and to predict possible values for the exponent B . To achieve this, we consider the size of the EQ, which refers to its spatial extent. From the distribution of the size and the dependence of moment on size, we derive the exponent of the GR law. In section 1, we present this relation, which will be of use all along this article. In section 2, we explore models with one-dimensional geometries and in section 3, we extend our approach to two-dimensional situations. In this geometry, we also propose an explanation for Omori-Utsu's law. A comparison of our results with existing theoretical results and with natural observations is presented in section 4. This article presents in detail the results announced in [8].

1. Relation between size and moment distributions

We consider models where space is discretized. The moment of an EQ writes $M = \sum_{i=1}^N \Delta x_i$, where Δx_i measures the total change of position of site i during the event and i ranges from 1 to N , with N being the number of sites involved in the event, i.e. the size of the event.

We first assume that the moment M is simply related to the size of the event N as

$$M \simeq N^\alpha, \quad (1)$$

where \simeq stands for equality up to a multiplicative constant. If the distribution of N is a power-law,

$$P_N(N) \simeq N^{-\beta}, \quad (2)$$

then the distribution of M is also a power-law

$$P(M) \simeq M^{-1-B}, \text{ with exponent } B = \frac{\beta - 1}{\alpha}. \quad (3)$$

This argument was previously introduced in [9] and used to constrain the admissible values of B .

This approach relies on the assumption of a single relation between M and N , such as equation (1). If we release this assumption and start with the general expression of a joint probability $P_j(M, N)$, a less strict condition for equation (3) to apply is that the joint distribution writes $P_j(M, N) = P_N(N) f(\frac{M}{N^\alpha}) N^{-\alpha}$. In other words, this means that the conditional probability of M given N is self-similar.

This argument relies on the existence of a relation between the moment M and a quantity N that we described here as the event size. The result remains valid if, instead of the size of the event, another quantity of the system is related to M as in equation (1) and is distributed as in equation (2). We shall, for instance, use this version of the result in the analysis of the standard Burridge-Knopoff (BK) model in section 2.1.

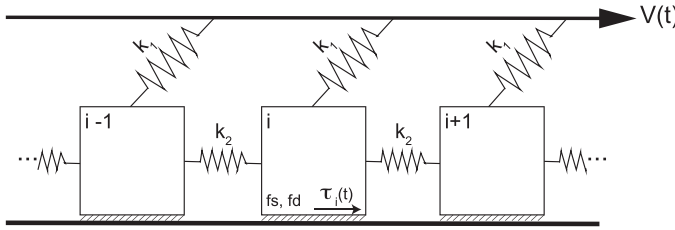


Figure 1. Schematics of the BK model. The i th block is pushed by its neighbors and the moving plate of speed $V(t)$.

2. One-dimensional models

2.1. Analysis of the Burridge-Knopoff (BK) model

We first consider the one-dimensional BK model, where a set of N_t sliders are located on a line at positions x_i , as illustrated in figure 1. Each slider is connected to its nearest neighbors with a spring of stiffness k_2 . The first and the last sliders are only connected to one neighbor. In addition, each slider is connected with a spring of stiffness k_1 to a plate moving at constant velocity denoted by v_0 .

The driving force on the i th slider is

$$\tau_i = -k_2(2x_i - x_{i+1} - x_{i-1}) + k_1(v_0 t - x_i). \quad (4)$$

When the sliders are all at rest, they experience a linear in time increasing load until this driving force τ_i reaches the static friction force F_s for a given slider i , which starts to move with velocity v_i and is then subject to the dynamic friction force

$$F_d(v_i) = F \frac{1 - \delta}{1 + \frac{2\Delta}{1-\delta} v_i} \quad (5)$$

where δ and Δ are positive constants. δ corresponds to the instantaneous stress drop from static friction to dynamic friction. As introduced in [10], the dynamic friction decreases as the slip velocity v_i increases. Such friction is referred to as velocity weakening friction, and Δ represents the amplitude of the negative velocity dependence. Then we are led to the equation of motion governing slider i ,

$$m \frac{d}{dt} v_i = \tau_i - F_d(v_i). \quad (6)$$

In addition, a slider is not allowed to move backward and if its velocity vanishes with a negative acceleration, the velocity is set to zero. We note that during the motion, the driving force applied to the neighbors of moving sliders increases and additional sliders can be put into motion.

Without loss of generality, we set to unity the masses of the movers, the stiffness k_1 , and the static friction force F_s . Unless otherwise stated, we use $N_t = 800$, $v_0 = 10^{-6}$, $\Delta = 10^{-3}$, $\alpha = 1$, and $k_2 = 9$ as is usually considered by former studies. We take for

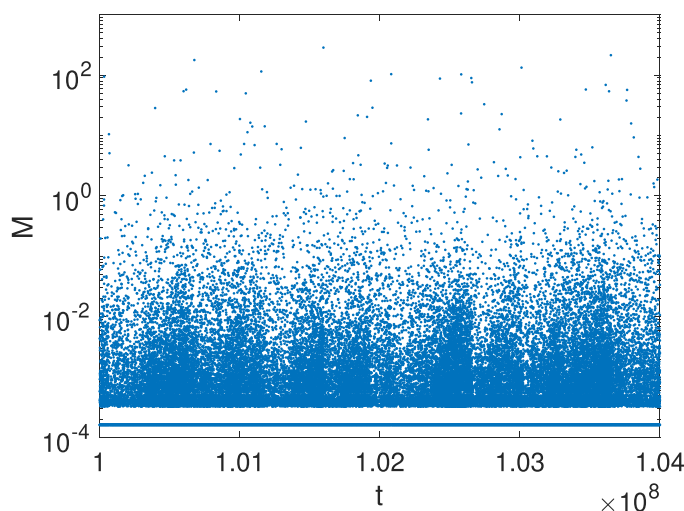


Figure 2. Moment M as a function of time of earthquake for the solution of the BK model with $N = 800$, $v_0 = 10^{-6}$, $\delta = 10^{-3}$, $\alpha = 1$, and $k_2 = 9$. Note both the existence of small events involving only one mass and with identical values of the moment (slightly smaller than 10^{-4}) together with events of moment that widely varies.

initial values of x_i small and uncorrelated random terms. For these parameters, the system alternates between a loading period during which the sliders are at rest and the driving force τ_i increases linearly in time and a brief event is initiated once one of the sliders starts moving and can put into motion a varying number of sliders. These sudden events are interpreted as the EQ in the BK model. The system has a chaotic behavior and in particular the size of the EQ fluctuates. The time series of the moment M of the events is displayed in figure 2. The PDF of the moment $P(M)$ is displayed in figure 3. As discussed in the introduction, the GR law corresponds to $P(M)$ being a power law. In this study, we focus on the behavior for large enough M , roughly spanning two decades between $M = 1$ and $M = 10^2$. Within this range of M , we measure a power-law exponent $1 + B = 1.56 \pm 0.1$.

To understand the origin of this behavior, we first discuss how events are formed. A crucial role is played by the stress field S_i , which we define as

$$S_i = -k_2(2x_i - x_{i+1} - x_{i-1}) - k_1x_i. \quad (7)$$

An EQ initiates at the site where S_i is maximum and at time t when S_i is equal to $F_s - k_1v_0t$. An example of stress profile just before an event is displayed in figure 4. It corresponds to an event that involves a large enough number of sliders. Going forward, we focus on such events with a number of moving masses $N \geq 30$. The general behavior is the following: the slider with maximum S_i value, the epicenter, starts to move and subsequently puts into motion its neighbor and this phenomenon propagates through a part of the system. We identified that an EQ can be partitioned into two spatial domains. An initial domain, that corresponds to stress values nearly equal to the maximum, see figure 4. For sliders within this domain, the total displacement at the end of the EQ,

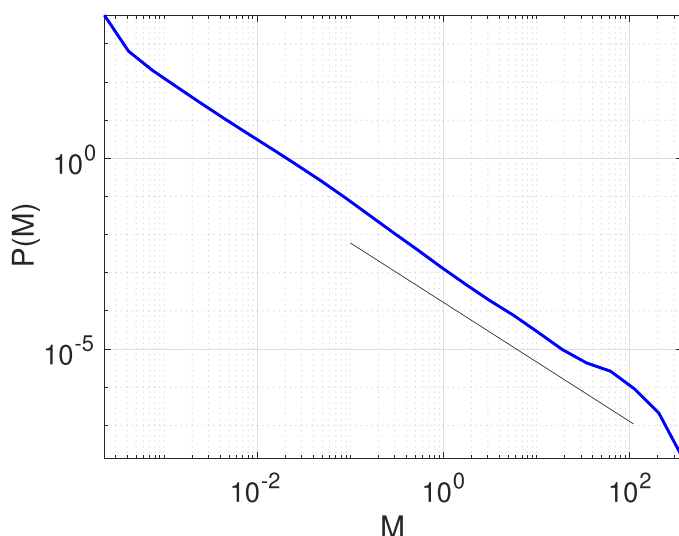


Figure 3. Distribution of the moment M for the BK model, with $N = 800$, $v_o = 10^{-6}$, $\delta = 10^{-3}$. For M between 0.5 and 113, a best fit leads to a power-law exponent $1 + B = 1.56 \pm 0.1$, indicated here as a straight line.

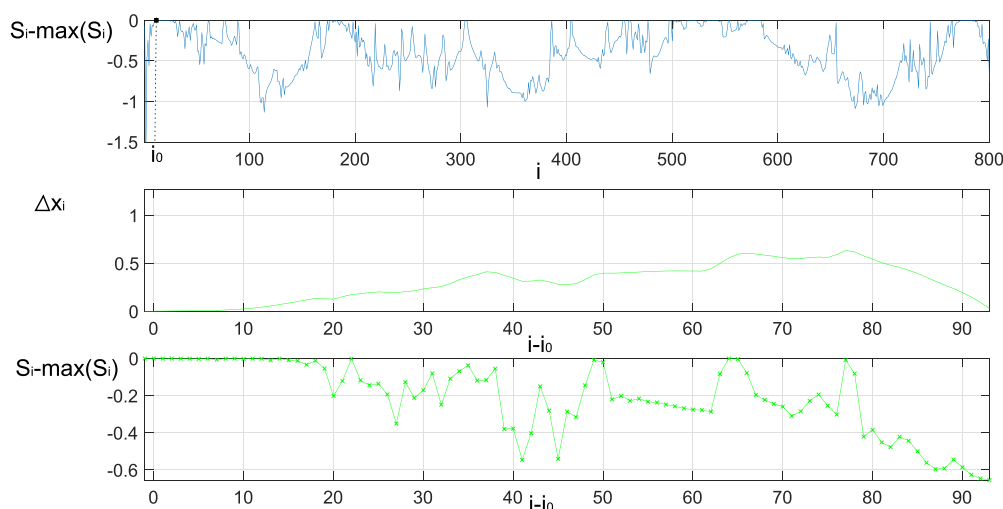


Figure 4. For the BK model, example of fields corresponding to an event involving $N = 95$ sliders. Top: stress profile before the event, i.e. value of S_i minus its maximum value as a function of i , the index of the 800 masses. The black square indicates the first moving mass (epicenter of position noted i_0). Middle: total slip as function of the position from the epicenter ($i - i_0$) for the event caused by the stress profile in the top figure. Bottom: zoom on the stress profile (same data as top figure) as function of the position from the epicenter ($i - i_0$). Note the initial phase for i smaller than 20 where S_i remains very close to its maximum.

Δx_i , scales as the square of the distance from the epicenter. This domain contains sliders close to the epicenter for which the difference between the stress and its maximum remains smaller than roughly $\Delta S = 0.2$. In the second domain, the slip depends on

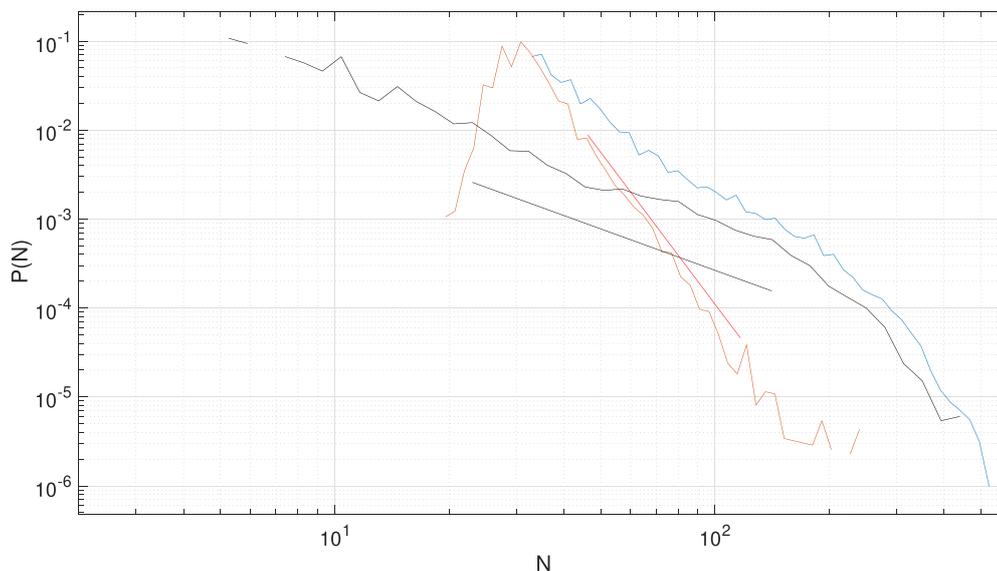


Figure 5. Distribution of size of earthquakes $P(N)$ for $N \geq 30$. Blue, total length N ; red, length of initial domain N_i and black, length of the second part of the EQ: $N_c = N - N_i$. The black straight line indicates the power-law with exponent $-\beta = -1.55 \pm 0.06$, obtained by a best fit for $23 \leq N_c \leq 140$, and the red straight line indicates slope -5.6 .

the initial stress. It increases with the distance from the epicenter if $\max(S_i) - S_i$ is smaller than ΔS . Otherwise, it decreases and a good qualitative description of the slip variation between neighboring sliders is that $\Delta x_{i+1} - \Delta x_i \propto (S_i - \max(S_i))$. The event terminates when the stress is such that Δx_i vanishes. This corresponds to the stress minus its maximum reaching large enough negative values for a sufficient number of masses.

A few comments are in order. We have just presented a simplified set of rules that, at least qualitatively, provide a description of the events. These rules rely on the value of the stress before the event and translate it into the spatial distribution of the slider slip once the EQ is over. We can only expect that this is valid in the regime of parameters that we are considering here and for specific events, for instance those involving a large enough number of sliders. Nevertheless, these rules allow us to obtain a statistically representative set of the real solutions of the BK model. In other words, the predictions derived from this simple set of rules correctly describe the properties of the BK model. Importantly, we stress that most of the detailed aspects have no influence for the prediction that we shall obtain.

We now turn to the statistical properties of the spatial extent of the EQ. We investigate both the size of the initial domain N_i , for which the initial stress S_i remains larger than its maximum minus ΔS and the size of the second part of the event, say N_c . The total size of an event is $N = N_i + N_c$. The distribution of N_i , N_c , and N are shown in figure 5. The initial phase has a peaked distribution that decreases at large N_i as either a power-law with large exponent (larger than 5) or as an exponential. In contrast, the distribution of N_c is wider and displays a power-law behavior with exponent

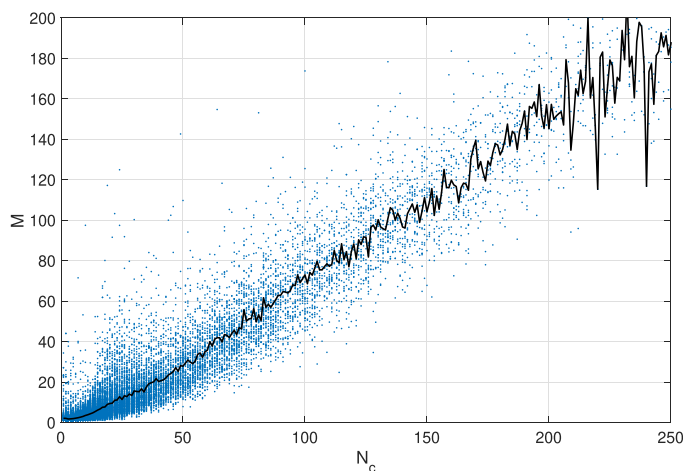


Figure 6. M versus N_c for events simulated by the BK model. Blue dots are individual events. The black curve is the moment M averaged over events at fixed value of N_c . Note the linear trend for large enough N_c .

$\beta = 1.55 \pm 0.06$. The distribution of N does not display a clear scaling domain. In summary, an event is characterized by two phases: an initial phase in which sizes do not fluctuate much and a second phase in which length N_c is more widely distributed, following a power-law of exponent β .

To conclude on this analysis of moment and length, we note that a relation between the moment of an event M and the length N_c exists and is shown in figure 6. For N_c larger than 10–20, the moment M is linear in N_c . This leads to an exponent $\alpha = 1$ for the law $M \simeq N_c^\alpha$ valid at large N_c .

Using the relation between M and N_c , we can now verify the relation obtained in equation (3). We found $\beta \simeq 1.55$, $\alpha \simeq 1$, thus $1 + (\beta - 1)/\alpha \simeq 1.55 \pm 0.06$, that is in nearly perfect agreement with the exponent $1 + B = 1.56 \pm 0.1$ obtained from the GR law.

To understand what controls the B -value, we have to understand what sets the value of α and β . $\alpha = 1$ implies that the moment is proportional to N_c . This is a simple consequence of the slip of each slider which is bounded and, more precisely, which fluctuates around a value roughly independent of N_c . This property is tested in figure 7, where events involving different numbers of sliders are plotted and no variations with N_c are observed.

To understand the value of β , we have to consider the condition for an event to stop. As discussed during the analysis of the stress profile, an event stops when the stress minus its maximum value reaches sufficiently negative values for a sufficient number of sliders. If we assume that S_i is a random walk, the probability to reach a given value for the first time after N_c steps is a power law which, if the steps of the random walks are uncorrelated, satisfies $P(N_c) \simeq N_c^{-3/2}$ [11]. We thus obtain from this argument an explanation for the value $\beta = 1.55 \pm 0.06$. The length of the EQ is $N = N_i + N_c$, where N_i does not fluctuate much whereas N_c is determined by the random walk behavior of the stress profile. Consequently, the distribution of N_c is a power-law with exponent $-3/2$.

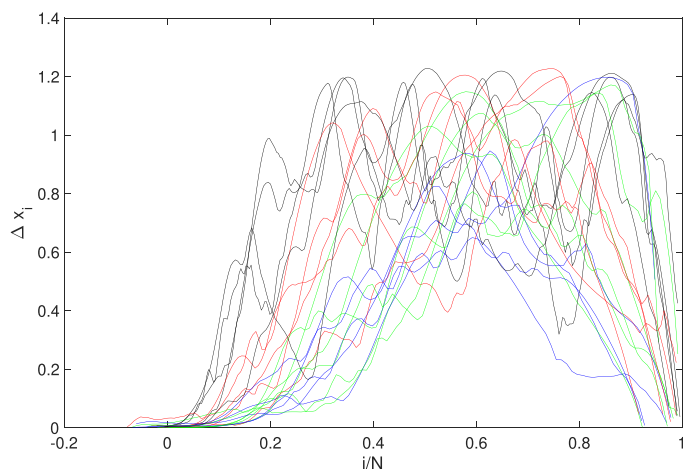


Figure 7. Slip as a function of the mass position normalized by the total number of masses involved in the event. Colors stand for different numbers of masses: Blue, between 80 and 100; Green, between 100 and 130; Red, between 130 and 170; and Black, above 170.

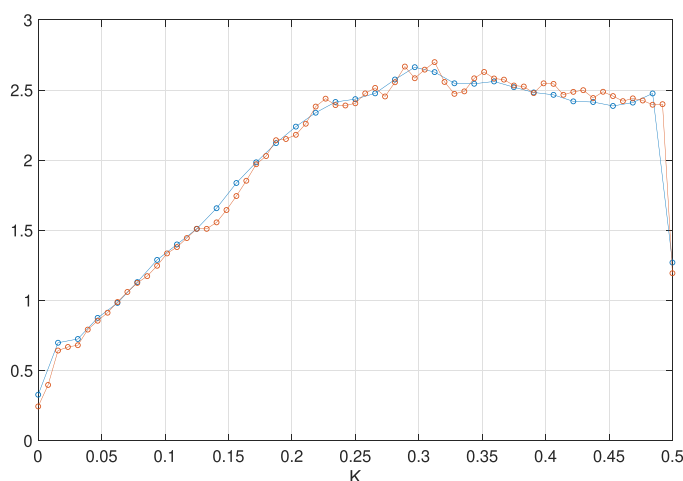


Figure 8. Power spectrum density of the spatial gradient of the stress profile before an event measured in the second part of the event and for events larger than $N = 64$ (blue) or $N = 128$ (red). The PSD tend to a non-zero value at vanishing wave vector K .

We can verify that S_i behaves as a random walk by calculating the power spectrum density (PSD) of its spatial gradient, see figure 8. The spectrum tends to a non-zero constant at small wavevector K , which implies that at large scale, S_i is indeed a random walk with uncorrelated increments.

In summary, our results on the BK model show that large enough events contain a large domain of size N_c , which is randomly distributed as $N_c^{-3/2}$, and reach slip values independent of N_c . These two properties constrain the B -value to $3/2$.

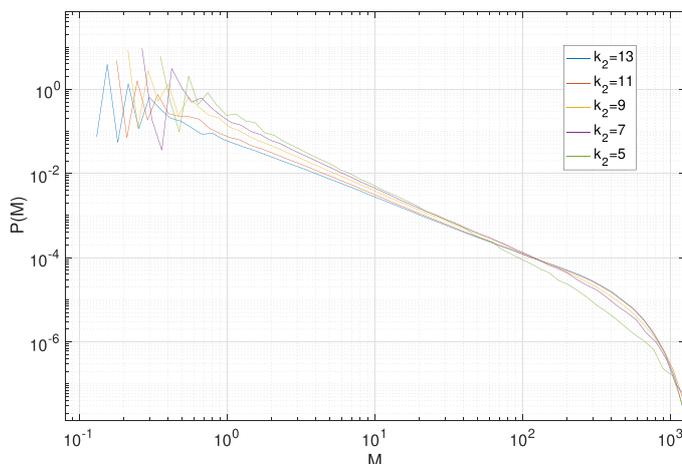


Figure 9. Probability density function (PDF) of the moment of the events M for the solution of the Coulomb friction model with $F_d = 0$, $N = 800$, $v_0 = 10^{-6}$, $k_1 = 1$ and varying k_2 (see color code in the legend).

2.2. Coulomb friction model

We now consider a modified version of the BK model in which the friction force can take only two values: the static friction force F_s or the dynamical friction force F_d . Both values are constant so that we name this model a Coulomb friction model. This model had been considered in the past [12] to study the effective friction force of an ensemble of sliders. Here, we focus on the distribution of magnitude. We consider the case $F_d = 0$ and choose the same values as in the standard BK model, $N = 800$, $v_0 = 10^{-6}$, $k_1 = 1$.

Despite the simplicity of this model, its solutions also display chaotic properties. We observe a wide distribution of the moment released at each event $M = \sum_i \Delta x_i$. Interestingly, these distributions display a power-law behavior $P \propto M^{-(1+B)}$, and the exponent B varies with k_2 (figure 9).

We also observe a wide distribution of the number of masses involved in each event N . As for the distributions of the moment, they display a power-law behavior $P \propto N^{-\beta}$, and the exponent β varies with k_2 , see figure 10.

In line with what we did on the standard BK model, we calculate the value of $\langle M \rangle_N$ where the average is taken at fixed value of N . At intermediate value of N , a power-law behavior $\langle M \rangle_N \propto N^\alpha$ emerges (see figure 11) and again the exponent α depends on the value of k_2 . Compared to our analysis of the standard BK model, we consider here the total length of each event. Indeed, for the events obtained for the Coulomb friction model, the initial phase observed in the standard BK model is not present. As a result, our analysis does not require us to remove the length of the initial phase of the earthquake in order to estimate the length of the critical zone. The argument is thus simpler for the Coulomb friction model.

This is also confirmed by analyzing the stress profile and its relation with the slip distribution. Unlike the standard BK model, the stress profile does not display a plateau near its maximum but rather isolated positions where the stress is close to its maximum. We observed that for events that involve a sufficient number of masses, there exists a

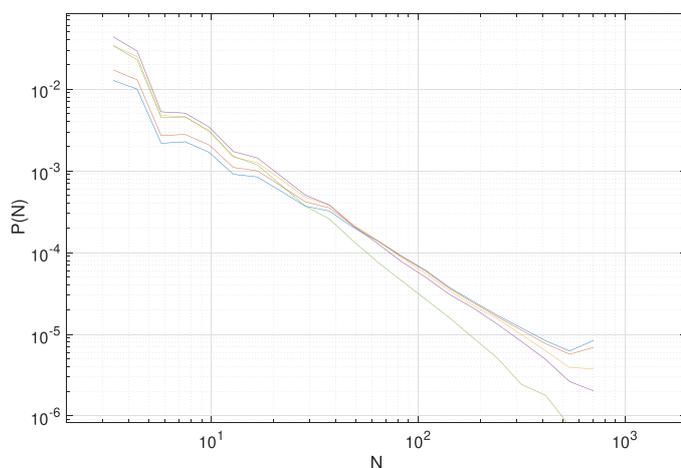


Figure 10. Probability density function (PDF) of the event size N for the solution of the Coulomb friction model and varying k_2 , same parameters and color code as in figure 9.

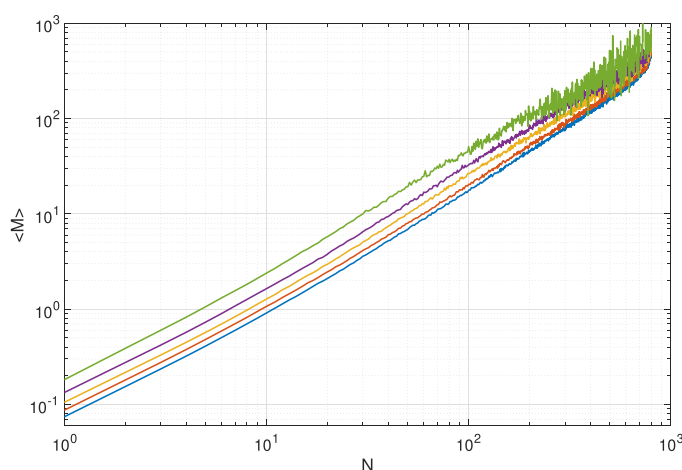


Figure 11. Moment M averaged over events of same size N for the solution of the Coulomb friction model and varying k_2 , same parameters and color code as in figure 9.

simple effective linear relation between S_i and Δx_i , so that the slip profiles correspond to excursions above a fixed threshold of the stress field.

Considering values of M and N for which the power-law behavior $\langle M \rangle_N \propto N^\alpha$ is observed, we calculate the values of the exponents α , β , B . They are displayed in figure 12 together with the prediction for the B -value: $B = (\beta - 1)/\alpha$. The prediction is verified.

To progress in the understanding of the B -value, we need to understand what sets the value of α and β . As the slip is roughly proportional to the stress profile, we can equivalently consider the stress profile. We thus calculate the PSD of the spatial gradient of the stress profile, which is displayed in figure 13. At small wavevector, $K < 0.1$, the spectrum displays a power-law behavior that we write as K^{1-2H} . We associate

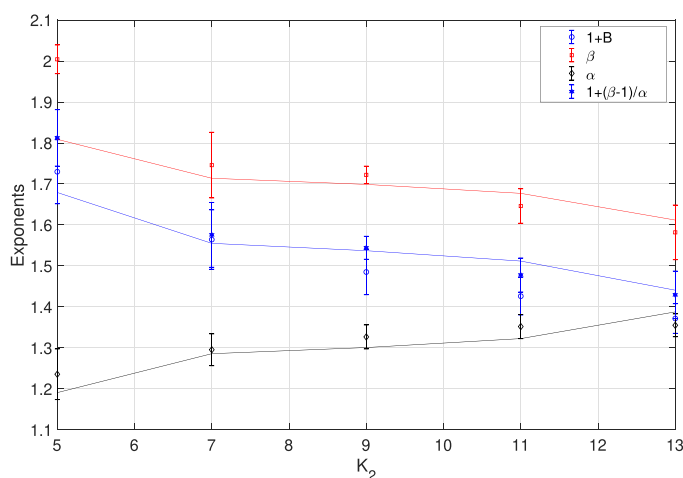


Figure 12. Exponents α , β , $1 + B$ and the prediction $1 + (\beta - 1)/\alpha$ as a function of k_2 for solutions of the Coulomb friction model. Symbols are best fits obtained for $2 \leq M \leq 100$ and $40 \leq N \leq 200$. Continuous lines are the predictions obtained from the fBm model ($\alpha = 1 + H$, $\beta = 2 - H$, $1 + B = 1 + (1 - H)/(1 + H)$) with H obtained by fitting the large scales of the spectrum of the gradient of the stress in figure 13.

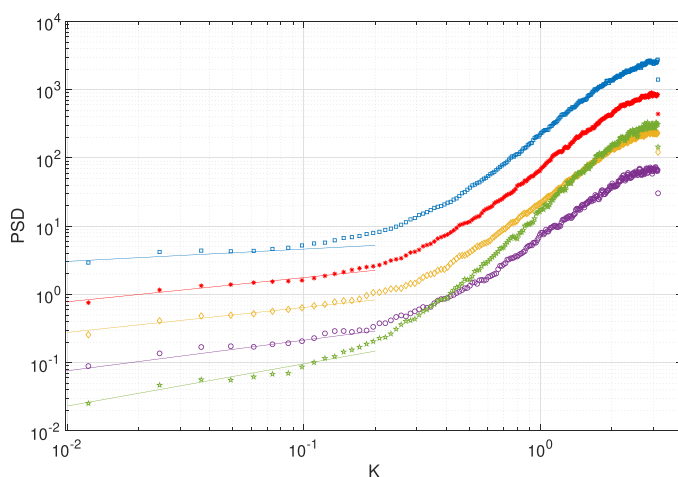


Figure 13. Power Spectrum Density of the spatial gradient of the stress S_i before events with $1 \leq M \leq 100$ and $80 \leq N \leq 170$. Straight lines are power-law fit for $K < 0.1$; the obtained exponents are $1 - 2H$, with H the Hurst exponent associated with the large scales of the stress profiles. Same parameters and color code as in figure 9.

this behavior to that of a fractional Brownian motion (fBm) of Hurst exponent H [13]⁵. Stated differently, the large scales of the stress profile are not trajectories of a standard Brownian motion as in the case of the BK model, but are excursions of a fBm.

⁵ The Hurst exponent is a characteristic of a fractional Brownian motion and it determines its roughness

Because the slip is proportional to the stress for the solutions of this model, we can use properties of the fBm to predict those of the earthquake. Return times of a fBm are distributed as $P(N) = N^{H-2}$ [14] so that the exponent for the EQ size is $\beta = 2 - H$. Typical excursions of a fBm of size N are of size N^H so that the area covered by a fBm excursion scales as N^{1+H} . This implies that the moment-size relation exponent is $\alpha = 1 + H$. We thus obtain a prediction for the B -value using the results of equation (3) as $1 + B = 1 + \frac{1-H}{1+H}$. This prediction, together with $\alpha = 1 + H$ and $\beta = 2 - H$, are displayed as continuous lines in figure 13, using H fitted from the spectrum of the gradient of the stress profile. A good agreement is found between the predictions and the results. This is quite satisfactory having in mind that α , β and B are calculated from the slip properties whereas H is measured independently from the stress profiles.

Let us sum up on the behavior of the Coulomb friction model. The large scales of the stress profile behave as a fBm of Hurst exponent H . The EQ slips are proportional to excursions of this fBm. This analogy between fBm and earthquake properties allows us to predict the values of the exponents α , β , and B as a function of one single parameter H , the Hurst exponent of the fBm.

2.3. Discussion

In these earthquake models, the underlying dynamics can be described in a simpler manner by considering the coupled dynamics of two fields. The first field is the stress before an event and the second field is the total slip during an event. We have identified that the stress field has scale-invariant properties, at least for a certain regime of EQ size. This stress field controls the dynamics of the EQ and the value of the slip of each event. In particular, the distributions of the lengths of the events also display power-law behaviors that result from the properties of the stress field. Together with the moment dependence on length, and using the relation between exponents given by equation (3), a prediction for the B -value is obtained. Essentially, the GR law finds its origin in the scale invariance of the stress profile.

What else can we learn from this approach?

Result 1 (R1)—It is generic and can be applied to other models of EQ (or of similar effects such as avalanches) in order to understand the origin of the self-similar behaviors.

R2—It provides a scheme to build other models of EQ. Such models would involve two steps, as sketched in figure 14:

First, the stress field sets the slip of the following event. In principle the stress field, together with the dynamical equations of continuum mechanics, allows us to calculate the slip. Our approach simplifies drastically the calculation of the slip. Other models of relation from stress to slip can be tested; we have for instance in mind a condition for the event to stop that would depend on the length of the event. Different conditions may lead to models with different properties, but we anticipate the existence of universality classes displaying the same statistical behavior and containing groups of different conditions for the termination of the EQ.

Second, the slip pattern modifies the value of the stress after the event. In principle, the slip spatial distribution together with the rules of equilibrium for continuum mechanics allow us to calculate the change of stress due to an EQ. In the models here, the

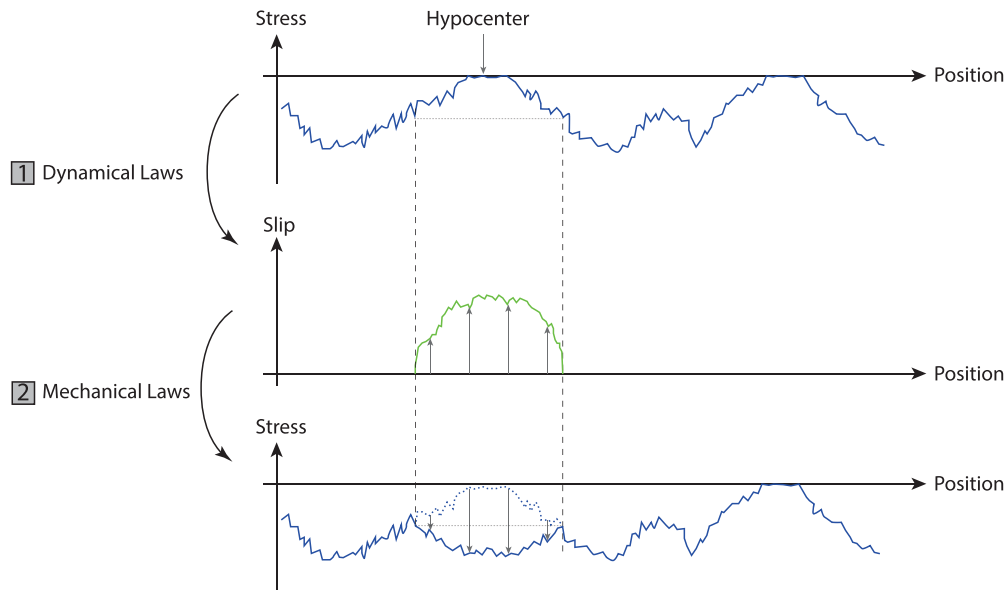


Figure 14. The two steps of evolution of the stress and slip profile. First: the stress profile determines what the slip is. Second: the slip profile changes the value of the stress. The iteration of this dynamic leads to a fixed point characterized by statistically stationary scale-invariant properties.

change is simply related to the motion of the sliders, through equation (4). Other rules may also be introduced to describe, for instance, the effect of material heterogeneity along the fault.

Using this methodology, a variety of models can be built and their properties be studied and compared to natural data. Again, as discussed for the EQ termination, we expect a limited number of asymptotic behaviors toward which will converge models having different rules for the EQ dynamics but belonging to the same universality class. We note that it is not uncommon in physics that different rules at small scales (here the scale of a slider) generate the same statistical behavior at large scales and long times.

R3—By analyzing separately these two steps, some understanding of their properties can be achieved:

The stress to slip problem can be seen as a non-standard application of random curves. The stress profile, a possibly correlated random trajectory defines through possibly nonlinear rules the slip distribution, which is also a random curve. This situation falls into the problem of random polymers: in the models studied here, a Brownian trajectory defines the stress field and we are interested in the excursion of the slip, which is a trajectory dependent on the Brownian. There exist some results for such problems which makes this analogy promising for both statistical mechanics and EQ modelling.

Here we reach conclusions using the properties of the return time of a Brownian or fBm. However, more complicated situations may occur, for instance if the stress is a Brownian motion while the slip is (case *a*) the integral of this Brownian motion or (case *b*) an integral of a function, f , of this Brownian motion. For case *a*, we expect that properties of the random acceleration process will be recovered. For case *b*, the law of

the return time of such processes is being studied by Berger *et al* [15]. For a Brownian motion, the distribution of the return length is shown to be a power-law as well as the distribution of the moment (the area below the curve). The value of the exponents depends only on the behavior of the function f for large values of its argument. In the case of a fBm, these statistical properties are largely unknown.

The second step in the modeling, from slip to stress field, is obviously crucial here. We still have little results on it: the stress field is, at least at large scale, self-similar but we do not know what determines its statistical properties, such as the Hurst exponent. This part of the problem belongs to the class of the evolution of random interfaces. The stress field changes at each event because of the EQ that decreases the stress of the moving sites and increases that of the neighbors. Yet, understanding how and when such a process lead to a self-similar stress profile remains a challenge. For this question also, very little is known, and it is possible that new classes of random interfaces will be identified. Recent work with N. P  tr  lis confirms the validity of this scenario and shows that the random addition of structures of variable size leads to self-affine interfaces.

It is likely that several properties result from the existence of large events with a power-law size distribution. For instance, in the solutions of the BK model, masses that participate in large events are more likely to have experienced a large event during their most recent motion. Large events, even though less likely to occur than smaller events, thus have a strong effect and affect the stress profile over long durations (i.e. on many iterations of the process). Whether this remains true in other models is an open question.

We believe that these two new classes of random trajectories and interfaces can be of interest for probabilists, and theoretical results are definitely lacking.

3. Two-dimensional geometry

The one-dimensional nature of the models considered so far makes it difficult to compare them with natural data. With the will to make use of what we learned so far, we now turn to two-dimensional (2D) systems, and we will follow the approach presented in the former discussion. First, we build a model (R2) and then analyze it (R3).

We could have considered an extension to 2D of the BK models that we considered in the former section but did not proceed as such and instead built a simpler model using the two steps as described in figure 14. Doing so, we will show that this two-step mechanism is indeed capable of generating an EQ-like series of events. In addition, its simplicity facilitates both its analysis and the generation of a sufficient quantity of data to obtain statistical convergence of the fluctuating quantities.

3.1. Description of the model

We consider a 2D geometry with N_i sites located on a square pattern. Between events, the stress at each site S_i increases linearly in time at a rate v_o . When the stress at one site, say i_0 , reaches a threshold value, S_c , an earthquake is initiated. Let D_1 be a constant stress threshold; we identify sites at which stress is larger than $S_c - D_1$. All these sites can be classified into clusters made of neighboring sites; see figure 15

for examples of stress fields. Only the sites which belong to the same cluster as site i_0 participate in the earthquake. Let N be the number of sites in this cluster. In line with the seismological observations [2], we assume that their total motion during the earthquake is proportional to \sqrt{N} which results in a moment $M = N^{3/2}$ and a magnitude $m = \log(M) = 3 \log(N)/2$.

The events are considered to be instantaneous compared to the inverse of the loading rate $1/v_0$. After an event, the stresses of the moving sites are set to new values equal to S_c minus a stress drop D_d equal to a constant D_2 plus a random term D_3 . The system has returned to its initial stage where the sites are at rest and the stress increases linearly in time.

A well-studied model in 2D, based on simple dynamical rules, is the OFC model [6]. Moving sites share their excess stress to neighbors and this leads to cascading events. This model has a quite rich behavior. It has now been pointed out that the frontiers of the system play an important role and in particular control the dynamics. Such systems are thus strongly inhomogeneous [3].

The model that we consider here uses a random term for the stress drop. We note D_3 as its amplitude and a random field is calculated with values of uniform probability between 0 and D_3 . The field is Fourier transformed in space, filtered by multiplication with a kernel K^{-s_n} , with K the wavevector, and then inversed Fourier transformed. This procedure generates a correlated random surface with Hurst exponent $H_n = s_n - 1$ [16]. The random field is calculated over all N_t sites but only the values corresponding to the moving sites are used. To save computational time, we perform this procedure only for events of size larger than 5; otherwise an uncorrelated random field is used with values uniformly chosen at random between 0 and D_3 . For $s_n = 0$, this procedure generates an uncorrelated random field (white noise), whereas for positive s_n , correlated fields are generated. The case $s_n = 1$, corresponding to independent increments, is named Gaussian free field [17]. In this model, the interaction between sites takes place when sites which belong to the same cluster move, and the value of the stress of these sites is reduced by a uniform value and a correlated value for $s_n \neq 0$.

Let us now sum up the three steps of this model:

- (1) Identify the site, say i_0 , with largest value of stress, say S_0 , and add a uniform stress $S_c - S_0$ to all the sites.
- (2) Find the clusters of sites whose stress is larger than the threshold $S_c - D_1$.
- (3) Change the value of the stress of the sites that belong to the same cluster as i_0 . The new values of the stress of these sites are $S_c - D_d$, where D_d is the sum of a constant and uniform stress drop, D_2 , and of a spatially dependant random term of amplitude D_3 .

3.2. Numerical results

Without loss of generality, we set $v_0 = 1$, $S_c = 1$, $D_1 = 1$. Numerical simulations are performed for $60^2 \leq N_t \leq 600^2$. We considered a constant field as initial condition or a randomly uncorrelated one. Statistical properties are calculated after a large enough initial transient so that they do not depend on the initial state. If D_2 is large enough

compared to D_1 , the system displays earthquake-like behavior with events that occur randomly in time and of random magnitude. If D_3 is small, the distribution of the moment is a power-law, like the GR law. More precisely, the PDF $P(N)$ displays a cut-off for $N \geq N_c$ and N_c increases either when D_3 decreases or N_t increases. We also note that at fixed N_t , for D_3 smaller than a threshold value, D_{3m} , the system shows nearly periodic behavior and loses the GR-like behavior. Our simulations show that D_{3m} decreases with N_t . To sum up, for large N_t , a GR law is observed provided $D_3 \ll D_1 \ll D_2$, i.e. the stress drop is large and its fluctuations are small compared to the threshold stress above which EQ are initiated. The inequality $D_1 \ll D_2$ implies that a long duration is necessary before a second event occurs at the same location, and $D_3 \ll D_1$ states that the stress drop after an earthquake displays small spatial variations compared to the stress threshold, itself smaller than the stress drop. These assumptions appear reasonable in the context of natural datas.

Nonetheless, our goal here is not to build a model encompassing every process occurring in nature. Rather, we search for simplicity instead and retain only the most essential effects. We shall see that the few effects that we keep are sufficient to explain both the GR law and Omori–Utsu’s law. We expect that more sophisticated models would also display these behaviors but that their origin would be the same as in the model considered here. Similarly, the ordering in the noise amplitude that is assumed here, $D_3 \ll D_1 \ll D_2$, may be released in other, more sophisticated models.

Unless otherwise stated, we will discuss results obtained with $D_2 = 10$, $D_3 = 0.1$, $N_t = 400^2$, $s_n = 0$ or $s_n = 1.5$. We display in figure 16 the time series of the size of the events $N(t)$. Large fluctuations are observed together with a clustering in time of the events that appears stronger for $s_n = 1.5$ than for $s_n = 0$.

The sizes of the events are distributed as a power-law, $P(N) \simeq N^{-\beta}$, see figure 17 with exponent β that depends on s_n . For $D_3 = 0.1$ and $s_n = 0$, a best fit for $3 \leq N \leq 80$ leads to $\beta = 2.046 \pm 0.015$. It decreases to $\beta = 1.93 \pm 0.01$ for $s_n = 1$ and $\beta = 1.63 \pm 0.01$ for $s_n = 1.5$. Results similar to those of $s_n = 0$ are obtained for small positive $s_n = 0.5$ or negative $s_n = -1$. In these models, the relation between size and moment is taken to be $M = N^{3/2}$, so that the B -values predicted by equation (3) are $B = 2(\beta - 1)/3$ and are respectively equal to 0.697, 0.62, and 0.42.

For what concerns the clustering of the events, we perform the following analysis. We consider events of size larger than 100 that we consider to be mainshocks. We then calculate the number of events per unit of time as a function of the time before or after the mainshock; this is displayed in figure 18 for $s_n = 0$ and $s_n = 1.5$. If we consider all events, an increase of EQ activity close to the mainshock is only visible for $s_n = 1.5$. If we restrict to events that are located at a distance smaller than 50 grid steps from the mainshock, then even the $s_n = 0$ case displays an increase of activity.

Measuring the unit of time with $\langle T \rangle$, the mean duration between EQ, we observe that the larger s_n , the stronger the increase of activity in the vicinity of the mainshocks, see figure 19. Both an Omori law (after the mainshock) and an inverse Omori law (before the mainshock) are visible. Displayed as a power-law in figure 20, different behaviors are visible depending on the duration of the mainshock. For each value of s_n , part of the data can be fitted using the standard Omori law, $\frac{dn}{dt} \propto (t + c)^{-1}$, see figure 21, but it

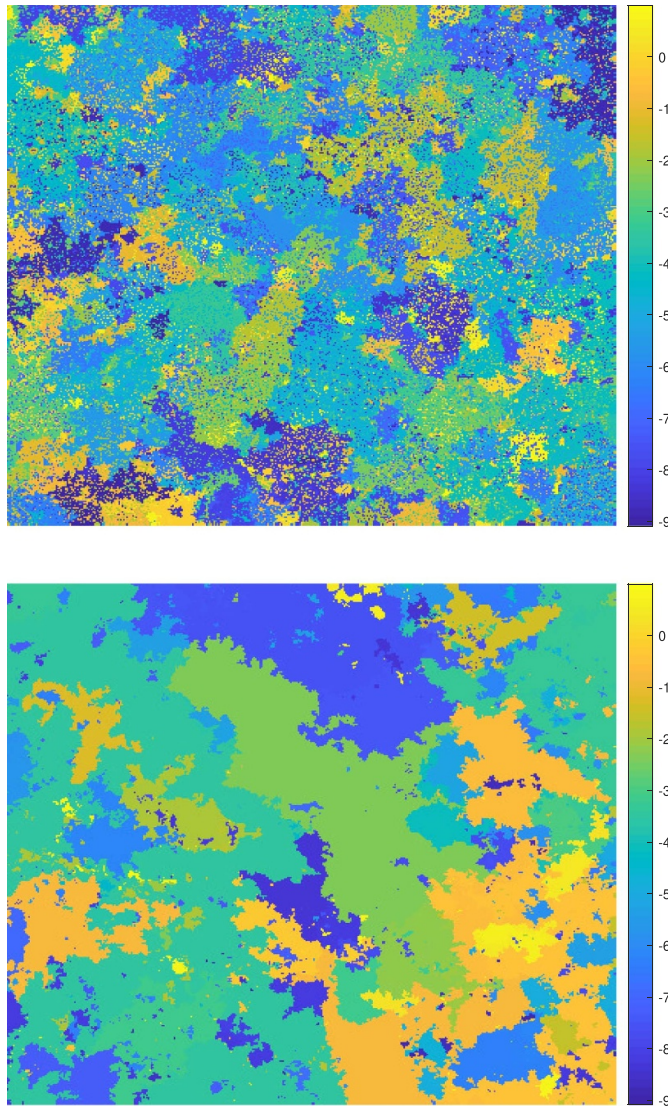


Figure 15. Snapshot of the stress field as a function of position for $D_1 = 1$, $D_2 = 10$, $D_3 = 0.1$, $N_t = 400^2$. Top, $s_n = 0$; bottom, $s_n = 1.5$. Values on the colorbar on the right.

is valid only on a restricted time interval so that the inverse-time expression provided by the Omori law is only a fit on part of the data.

3.3. Discussion

3.3.1. The stress as a random surface and results from percolation theory. The observed behavior can be understood by an analysis of the spatial distribution of the stress. The stress field is a surface and events involve clusters of sites for which the stress is above a threshold value. This problem is classical in statistical physics, as it covers a variety of analogous situations [18]. The stress can be considered as a topography that

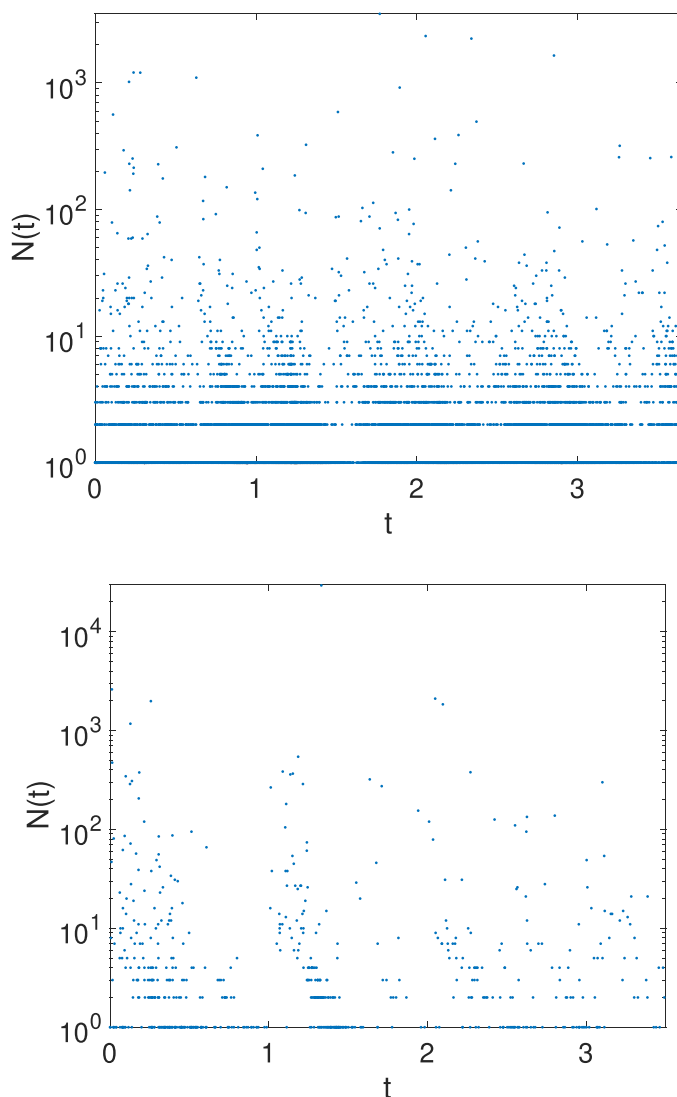


Figure 16. Time series of EQ size $N(t)$ for the 2D model for $D_1 = 1$, $D_2 = 10$, $D_3 = 0.1$, $N_t = 400^2$. Top, $s_n = 0$; bottom, $s_n = 1.5$.

is filled with water until a given altitude, and we are interested in the size of the islands or continents [19]. If the comparison of the stress with a fixed threshold amounts to define whether a site is occupied or empty, then the problem of percolation is recovered [20].

Indeed, random surfaces and the properties of clusters above a cut belong to the universality class of percolation, possibly over a correlated disorder. More precisely, provided some mild hypothesis on the random surface, there exists a threshold at which the system is critical and displays properties alike to those of percolation. In particular, close to the critical point, cluster sizes are distributed following a power-law with exponent τ_F , the so-called Fisher exponent. If the heights h of the surface at different positions are uncorrelated, standard percolation takes place and $\tau_F = 187/91$ [20].

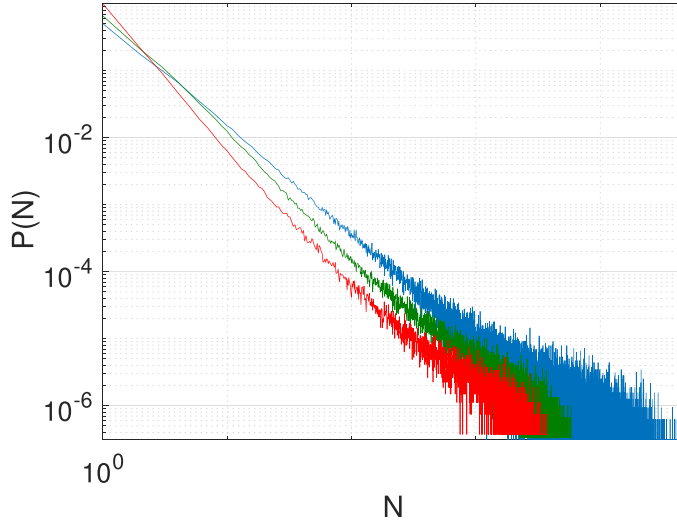


Figure 17. PDF of EQ size $P(N)$ for the 2D model for $D_1 = 1$, $D_2 = 10$, $D_3 = 0.1$, $N_t = 400^2$. Red, $s_n = 0$; green, $s_n = 1$; blue, $s_n = 1.5$.

If the height is Gaussian and correlated as $\langle (h(x+R) - h(x))^2 \rangle^{1/2} = R^H$, then correlated percolation takes place. We note that another way to quantify correlations is to use the PSD of the field h . In 2D, the PSD behaves as $S(K) \propto K^{-2-2H}$. It has been shown in [18, 21] that for $H \leq -3/4$, correlations do not affect the critical behavior that remains identical to that of uncorrelated percolation. For $-3/4 \leq H$, the critical exponents vary with H .

We have calculated the spectrum of the stress field, see figure 22. We observe for the set of parameters considered here ($D_1 = 1$, $D_2 = 10$, $D_3 = 0.1$, $N_t = 400^2$) that the spectrum behavior depends on s_n . For $s_n = 1.5$, i.e. $H_n = s_n - 1 = 0.5$, we have a clear power-law behavior of the exponent around -1.35 . For $s_n = 1$, $H_n = 0$, a power law of exponent closer to -1 is observed on a slightly narrower range of K . For $s_n = 0$, any power-law behavior would be restricted to a quite narrow range, so that it appears more accurate to describe the behavior of the spectrum as asymptotically constant at small and large K and gently transitioning between the two values at intermediate K . We stress that the exponent of the spectrum, equal to $-2 - 2H$ with H the Hurst exponent of the surface, varies with the exponent s_n of the noise term, but in a non trivial manner. For the values reported here, we have $H \simeq -1$, -0.5 , and -0.32 respectively for $H_n = -1$, 0 , and 0.5 . Indeed the stress field results from the repeated addition of noise terms of fluctuating size so that it is not surprising that its behavior differs from the one of a single stress drop.

3.3.2. The GR law and the b-value. The observed properties can be understood by considering that the stress field has the same properties as a random field with an Hurst exponent H that depends on s_n . As a consequence, we expect that the distribution of size of clusters above a threshold follows a power-law of exponent τ_F . This is in agreement with the exponent of the size distribution of the events for small s_n , as we have measured $\beta = 2.046 \pm 0.015$ for $s_n = 0$, very close to Fisher prediction for uncorrelated

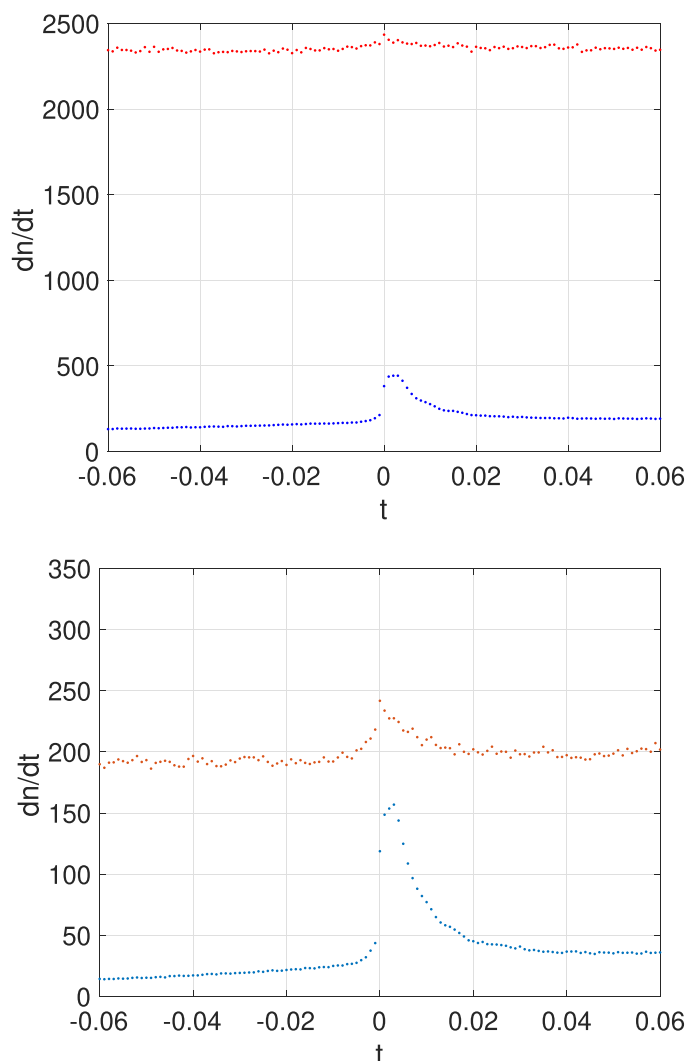


Figure 18. Averaged number of events per unit of time as a function of duration to a main event of size $N \geq 100$. Red: $s_n = 0$ and blue: $s_n = 1.5$. Top: all events considered. Bottom: only events with epicenter located from the main shock at a distance smaller than 50 are considered.

percolation $\tau_f = 187/91 \simeq 2.055$. For positive s_n , a smaller exponent is measured that can be ascribed to correlations in the stress field, so that predictions from uncorrelated random percolation do not apply. If the stress surface has strong correlations, namely $H > -3/4$, the analogy with correlated percolation predicts a decrease in the B -value. This is indeed observed in our model as $B = 0.697$ for $H = -1$ ($s_n = 0$) and the same value is obtained within error bars for $s_n = -1$ and $s_n = 0.5$, thus with moderate correlations. Increasing the correlation and for H above $H = -3/4$, we measure as expected a decrease in B since $B = 0.62$ for $H = -0.5$ and $B = 0.42$ for $H = -0.32$. We also note that the measured exponent can depend on the noise amplitude. Indeed, at larger noise, a peak at large N appears which in turn modifies the slope of the PDF of N even at

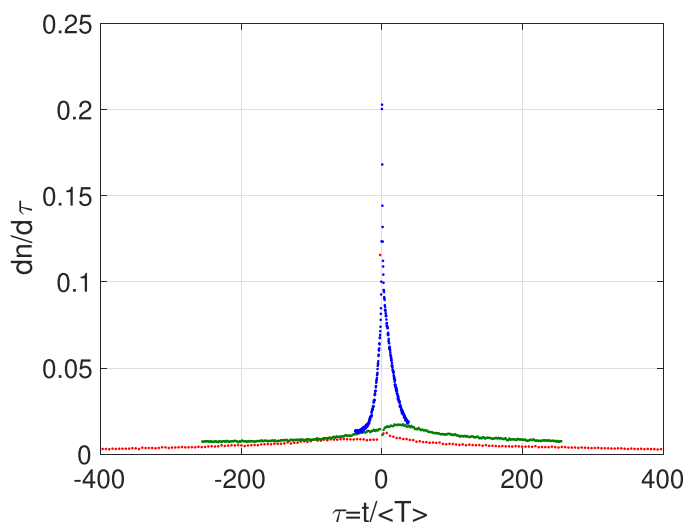


Figure 19. Averaged number of events per unit of time as a function of duration to a main event of size $N \geq 100$. Only events of size larger than 10 and with epicenter located from the main shock at a distance smaller than 50 are considered. Time is measured in unit of the mean interevent duration. Red, $s_n = 0$; green, $s_n = 1$; and blue, $s_n = 1.5$.

smaller value. This, together with finite size effect, may lead to an apparent exponent different from the true power-law behavior.

Written in term of b -values, this analysis predicts $b = 96/91 \simeq 1.05$ and $B = 64/91 \simeq 0.70$ for weakly correlated stress surfaces. If the stress surface has strong correlation, we expect a decrease in these values. This is compatible with most reported natural values [2, 3].

3.3.3. Existence of aftershocks and the Omori-Utsu law. Aftershocks and foreshocks are also explained by the spatial structure of the stress field. Correlated random surfaces display level sets that are spatially correlated. More precisely, if a domain has a large value of stress, other clusters with large stress are likely to be located in its vicinity. This property of random surface has, to the best of our knowledge, not been described. We have simulated random surfaces with various exponents H by multiplication in Fourier space with a well-chosen power-law [16]. Examples are displayed in figure 23 where the correlated random surface displays clustering in space of its level set. To quantify this effect, we have simulated a large number of random surfaces. For each surface, we identify the sites whose value is above a given threshold. The value of the threshold sets the value of the probability p of occupation of a site in the framework of percolation theory. We then identify the clusters of connected sites. We next calculate the distance d between the largest cluster and any other cluster. The distribution of the distance is a characteristic of the spatial organization of the clusters. It is displayed in figure 24 for different values of p and H . Compared to uncorrelated surfaces, the correlations induce a non-homogeneous localization of clusters with respect to the position of a given cluster.

Stress spatial distributions, the Gutenberg-Richter and the Omori-Utsu laws

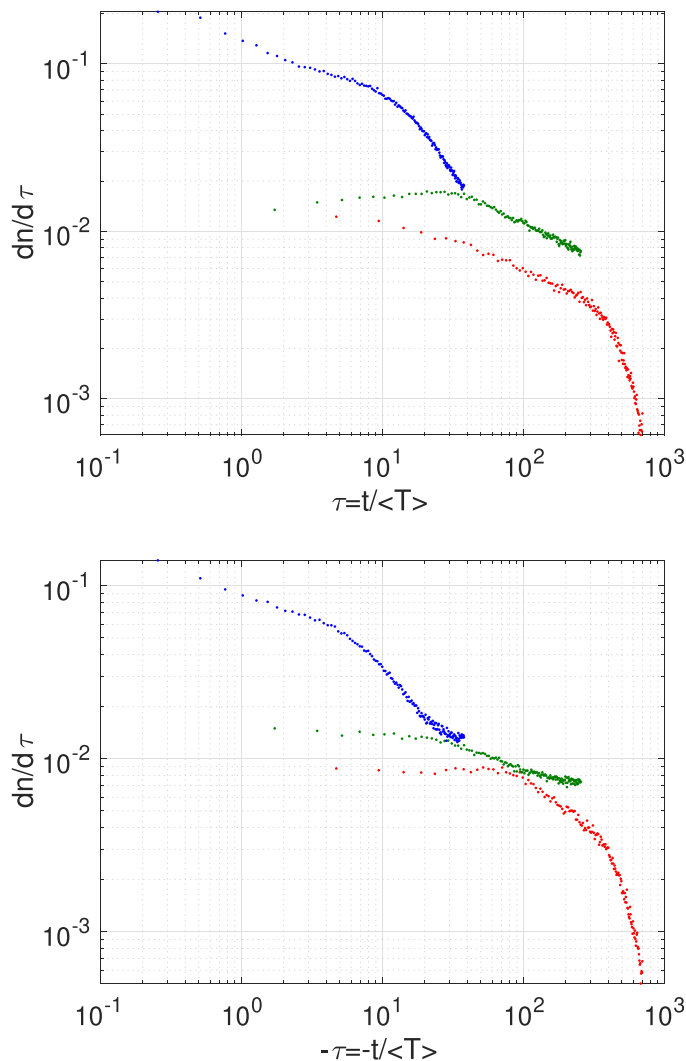


Figure 20. Log-log plot of the same data as in figure 19, for (top) aftershocks, and (bottom) foreshocks.

We conclude that clustering in space of individual clusters with large stress is a consequence of the geometrical properties of the stress field that behaves at large scale as a correlated random surface. This provides an explanation for the existence of aftershocks: close to a mainshock, there exist clusters where stress is large and close to initiate an EQ. This mechanism is purely geometrical and does not require additional phenomena (stress transfer, pore pressure dynamics, viscosity, etc.).

For what concerns the rate of aftershocks, as mentioned in the section analysis of the results, the Omori law is only a fit on part of the time series. We plan to investigate further if this can be deduced from the properties of clusters in percolation theory.

We ended section 2 on the 1D models by mentioning the need for additional studies on these new problems of random curves and interfaces. The same remarks apply for the

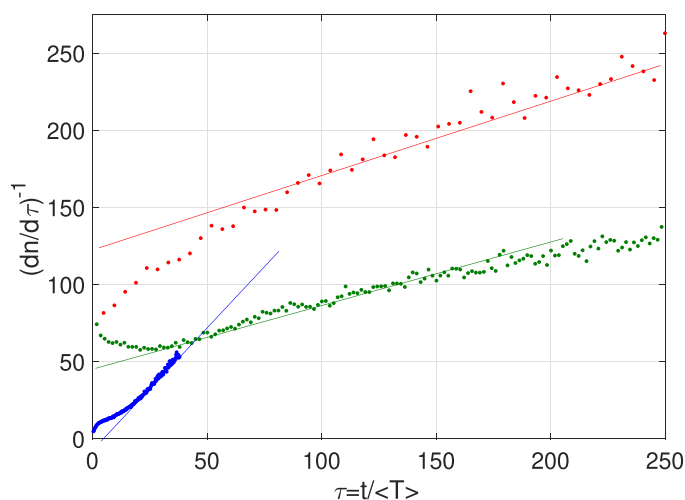


Figure 21. Inverse of the averaged number of events per unit of time as a function of duration to a main event of size $N \geq 100$. Only events of size larger than 10 and with epicenter located from the main shock at a distance smaller than 50 are considered. Time is measured in unit of the mean interevent duration. Red, $s_n = 0$; green, $s_n = 1$; and blue, $s_n = 1.5$. Same data as in figure 19. Straight lines are guide for the eyes and correspond to the Omori law.

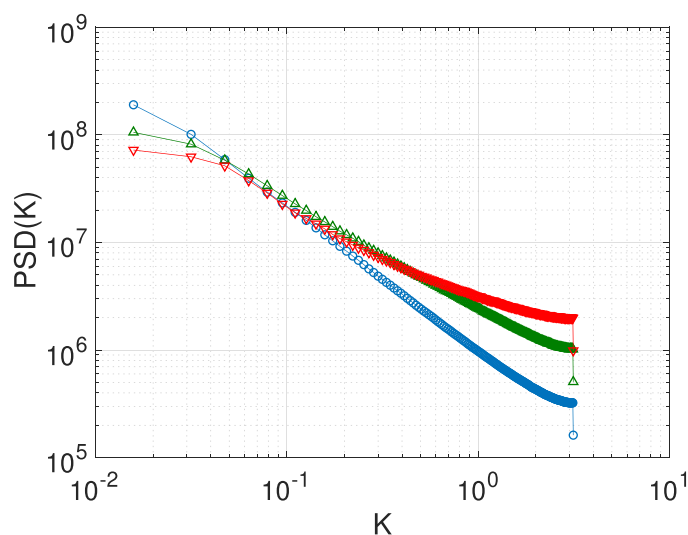


Figure 22. Power spectrum density of the stress field $S(K)$. Red, $s_n = 0$; green, $s_n = 1$; blue, $s_n = 1.5$.

2D case. Statistical properties of random surfaces built upon a 2D random stress profile (the 2D version of the polymer approach) and properties of random 2D dynamically evolving interfaces are topics that have called for very little attention.

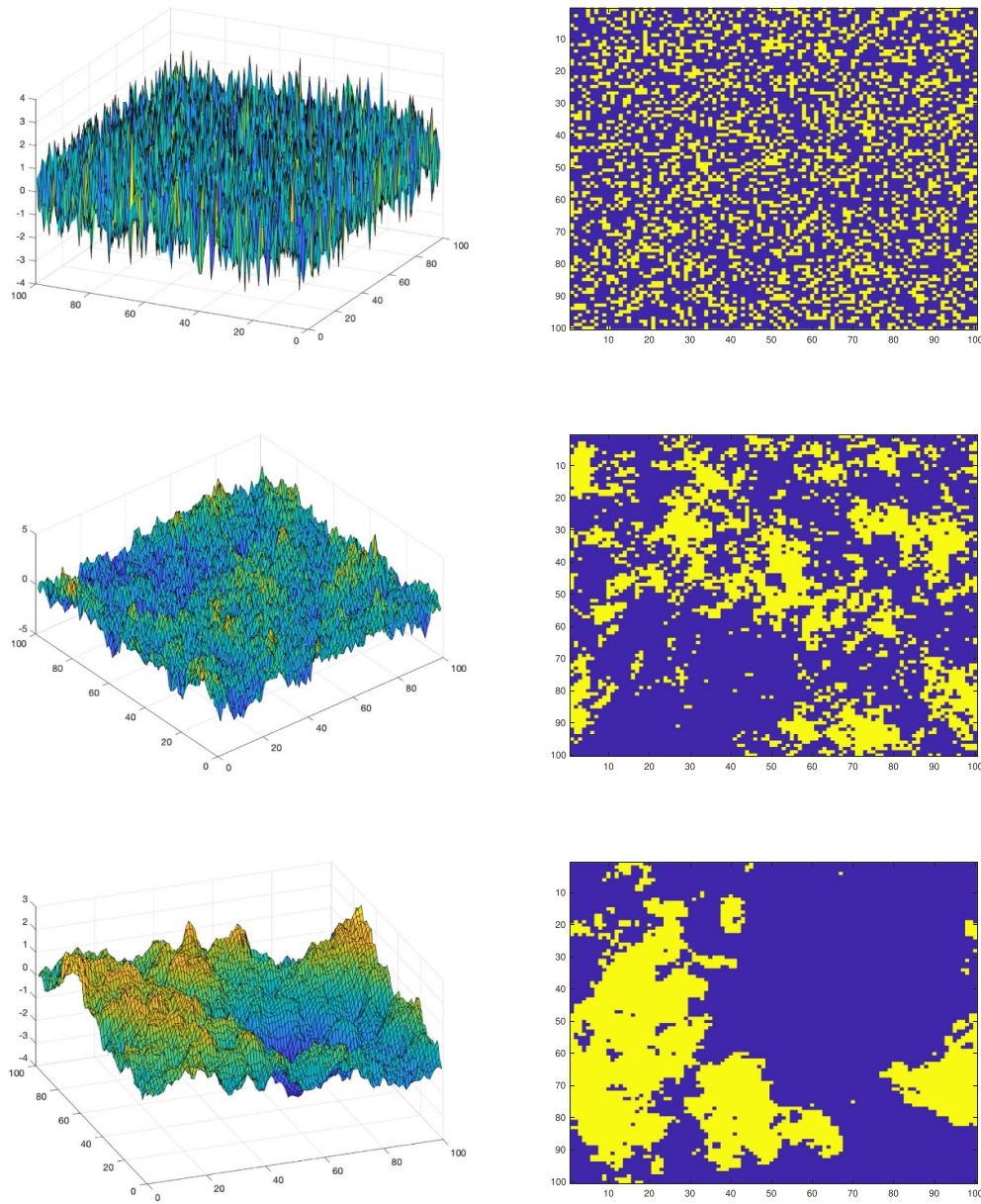


Figure 23. Random surfaces calculated with, from top to bottom, $s_n = 0$, $s_n = 1$, and $s_n = 1.5$. Left: value of the field as a function of space. Right: sites with value higher than a fixed threshold so that 0.3 of the sites are above the threshold. Note that the larger the s_n the more localized in space are the clusters.

4. Discussion

4.1. Comparison with theoretical results

We compare the results presented here with some previous publications. While the relation between exponents equation (3) is mentioned in [9], it has not been validated

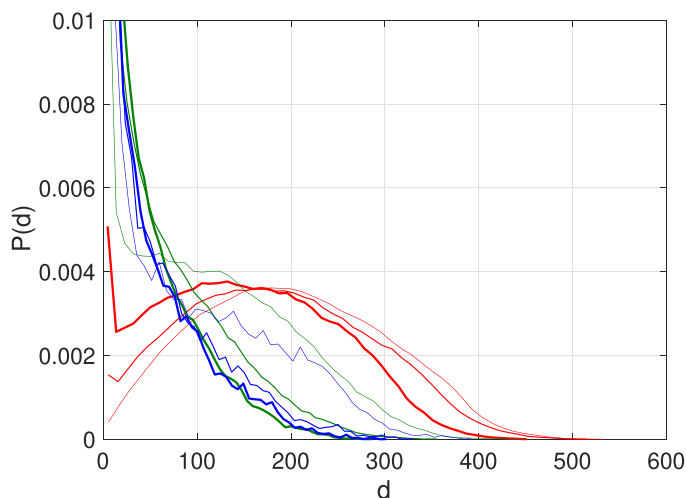


Figure 24. Probability density function of the distance d between the largest cluster and the other clusters for a random surface with exponent $s_n = 0$ in red, $s_n = 1$ in green, and $s_n = 1.5$ in blue. The fraction of sites belonging to clusters increases with the line thickness and is 0.3, 0.5, and 0.55. The total number of sites is 400^2 .

against existing data. Similar relations have also been used to assess scaling laws in the EQ community; see for instance [22]. The generalization to the case of a self-similar joint distribution of moment and size, and the application to the case where a different quantity than the size is considered, are both new results.

Relating the GR law to some fault fractal properties has been proposed in [23] and [24]. In the latter, a field property is assumed to be a fractal, and statistical properties of their level set are used. Recent tests using data in boreholes are presented in [25], where the self-similar nature of the elastic properties of the fault material are considered. Our work, in contrast, identifies the origin of the self-similar property: it is a consequence of the repeated effects of all former events. Our results also include a prediction for the values of several exponents, including the b -value. These exponents depend on the field similarity exponent, as is shown by the analogy with percolation.

It has been proposed that the EQ belong to the class of self-organized critical systems (SOCs). The idea is that such systems evolve spontaneously towards a critical point [26]. The models presented in this article all require either fine tuning of their parameters (for the 1D model such as the standard BK model) or a large difference of amplitude between the parameter values (for the 2D model). If other parameters are selected, the GR law is not observed. In that sense, these models are not spontaneously evolving towards a critical point.

We also note that self-similarity of the stress (long-range correlation or, similarly, power-law behavior of its power spectrum) do not necessarily have to be in the vicinity of a critical point. Processes based on a random walk or a fractional random walk can

result in a power-law behavior in 1D. and the appearance of such random walks does not require a critical phenomenon. This is the case in the 1D models studied in section 2.

In the model in 2D, the percolation critical point plays a role and selects the exponent of the distribution of the cluster size. This is true for the regime considered here with negative H (Hurst exponent of the stress field). For positive H , the percolation transition disappears and yet the cluster sizes also follow a power-law distribution [19]. This is another example of a system in which a power-law behavior occurs on an extended domain of parameters and not only at a critical transition.

Based upon the idea of SOC, a model named OFC was studied in [6]. As our model in 2D, it is a cellular automaton with simple dynamical rules. It has been shown that the properties of this model are in part controlled by the location of the earthquake epicenter [3]. They nucleate close to the system boundaries, and changing the control parameters modifies the extent of their spatial localization. The lack of homogeneity due to the specific role of the boundaries renders it difficult to analyze in the framework presented in this article.

Regarding aftershocks, our study shows that the self-affine property of the spatial distribution of the stress is sufficient to explain the existence of aftershocks. Obviously, other effects prone to trigger aftershocks could also be involved in nature and contribute to the aftershock sequences. We note that the simpler version of the BK models in 1D and 2D do not display aftershock sequences, see discussion in [3]. In a 2D model with heterogeneous friction properties, a viscoelastic coupling to the asthenosphere would create aftershocks that verify the Omori law [27]. More recently, a model of fault based on the coupling between a velocity weakening elastic layer and a viscoelastic velocity strengthening layer is able to recover statistical properties of aftershocks as observed in nature [28]. It would be interesting to investigate in these models whether the stress spatial structure becomes self-affine when the viscous effects play a role which would provide a simple explanation for the origin of the aftershocks.

4.2. Comparison with natural data

There exists only few studies on the stress distribution in nature. Some studies have shown that the topography of faults are self-affine with their roughness associated to an Hurst exponent of order 0.2–0.8 [29]. Interestingly, evidence suggests that the slip itself scales with a Hurst exponent close to 0.6. Using a 3D fault numerical model it was predicted that the frictional stress field scales with an Hurst exponent of -0.4 [30]. In line with our description of slip and stress, several fields in nature display large scale behaviors that are self-similar.

For what concerns the b -value, we predict $b = 96/91 \simeq 1.05$ for weakly correlated stress field and a smaller one for strong correlation, which is compatible with most reported natural values [2, 3]. Some studies report a variation of b with properties of the faults, in particular on the nature of the fault and thus on its stress [31, 32]. Our work provides an explanation for these effects: fault properties influence the self-affine behavior of the stress field or the moment–size relationship. These properties, in turn, modify the b -value. We add that in a recent experiment of sheared granular matter, the

authors report $B = 0.71 \pm 0.01$ for the released energy during the events [33], which is in perfect agreement with our prediction $B = 64/91 \simeq 0.70$.

We hope that further studies on the stress in the vicinity of a fault will investigate the possibility of a self-affine behavior. It would also be interesting to analyze natural data in terms of level sets of random surfaces. In particular, some specific properties of clusters can be tested (fractal dimension, typical shape, etc). The spatial clustering of events should also be compared to that of level sets of random surfaces, and indicators of proximity of a large event might be obtained in this framework.

Acknowledgments

F P gratefully acknowledges the Visiting Research Program in 2019 at the Earthquake Research Institute, the University of Tokyo, and the IEA action of CNRS. A S gratefully acknowledges the support of the European Research Council Grant REALISM (2016-Grant 681346). T H acknowledges grants from the MEXT Program, Data Creation and Utilization Type Material Research and Development Project No. JPMXP1122684766 and KAKENHI Program Nos. JP21H05201 and 22H01145.

References

- [1] Scholz C H 2019 *The Mechanism of Earthquakes and Faulting* (Cambridge University Press)
- [2] Kanamori H and Brodsky E E 2004 *Rep. Prog. Phys.* **67** 1429
- [3] Kawamura H, Hatano T, Kato N, Biswas S and Chakrabarti B K 2012 *Rev. Mod. Phys.* **84** 839
- [4] Utsu T, Ogata Y and Matsu'ura R S 1995 *J. Phys. Earth* **43** 1–33
- [5] Burridge R and Knopoff L 1967 *Bull. Seismol. Soc. Am.* **57** 341
- [6] Olami Z, Feder H J S and Christensen K 1992 *Phys. Rev. Lett.* **68** 1244–8
- [7] Carlson J M, Langer J S and Shaw B E 1994 *Rev. Mod. Phys.* **66** 657
- [8] Pétrélis F, Chanard K, Schubnel A and Hatano T 2023 *Phys. Rev. E* **107** 034132
- [9] Vasconcelos G, de Sousa Vieira M and Nagel S R 1991 *Phys. Rev. A* **44** R7869(R)
- [10] Carlson J M, Langer J S, Shaw B E and Tang C 1991 *Phys. Rev. A* **44** 884
- [11] This is a well-known property of random walk. For a mathematical approach, see Feller W 1968 *An Introduction to Probability Theory and Its Applications* (Wiley Series in Probability and Mathematical Statistics vol 1) (Wiley)
- [12] Kiss T, Janszky H J and Adam P 1994 *Phys. Rev. E* **49** 4935
- [13] Mandelbrot B and Van Ness J W 1968 *SIAM Rev.* **10** 422–37
- [14] Ding M and Yang W 1995 *Phys. Rev. E* **52** 207
- [15] Berger Q and Béthencourt L 2023 An application of Sparre Andersen's fluctuation theorem for exchangeable and sign-invariant random variables (arXiv:2304.09031)
Berger Q, Béthencourt L and Tardif C 2023 Persistence problems for additive functionals of one-dimensional Markov processes (arXiv:2304.09034)
- [16] de Castro C P, Luković M, Andrade R F S and Herrmann H J 2017 *Sci. Rep.* **7** 1961
- [17] Lodia A, Sheffield S, Sun X and Watson S S 2016 *Probab. Surv.* **13** 1–56
Duplantier B *et al* 2017 Log-correlated Gaussian fields: an overview *Geometry, Analysis and Probability* (Progress in Mathematics vol 310) ed J B Bost, H Hofer, F Labourie, Y Le Jan, X Ma and W Zhang (Birkhäuser)
- [18] Ishenko M B 1992 *Rev. Mod. Phys.* **64** 961
- [19] Olami Z and Zeitak R 1996 *Phys. Rev. Lett.* **76** 247
- [20] Stauffer D and Aharony A 2010 *Introduction to Percolation Theory* (Taylor and Francis)
- [21] Zierenberg J, Fricke N, Marenz M, Spitzner F P, Blavatska V and Janke W 2017 *Phys. Rev. E* **96** 062125

- [22] Romanowicz B 1992 *Geophys. Res. Lett.* **19** 481–4
- [23] Aki K 1981 A probabilistic synthesis of precursory phenomena *Earthquake Prediction (Maurice Ewing Series vol 4)* ed D W Simpson and P G Richards (American Geophysical Union) pp 566–74
- [24] Huang J and Turcotte D L 1988 *Earth Planet. Sci. Lett.* **91** 223–30
- [25] Langenbruch C and Shapiro S A 2014 *J. Geophys. Res. Solid Earth* **119** 1220–34
- [26] Bak P, Tang C and Wiesenfeld K 1987 *Phys. Rev. Lett.* **59** 381–4
- [27] Pelletier J D 2000 *Geocomplexity and the Physics of Earthquakes (Geophysical Monograph Series vol 120)* (American Geophysical Union (AGU)) p 27
- [28] Petrillo G, Lippiello E, Landes F P and Rosso A 2020 *Nat. Commun.* **11** 3010
- [29] Renard F, Candela T and Bouchaud E 2013 *Geophys. Res. Lett.* **40** 83–87
Abe S and Deckert H 2021 *Solid Earth* **12** 2407
Bruhat L, Klinger Y, Vallage A and Dunham E M 2020 *Geophys. J. Int.* **220** 1857–77
- [30] Candela T, Renard F, Schmittbuhl J, Bouchon M and Brodsky E E 2011 *Geophys. J. Int.* **187** 959–68
- [31] Schorlemmer D, Wiemer S and Wyss M 2005 *Nature* **437** 539–42
- [32] Scholz C H 2015 *Geophys. Res. Lett.* **42** 1399–402
- [33] Lherminier S, Planet R, Levy dit Vehel V, Simon G, Vanel L, Måløy K J and Ramos O 2019 *Phys. Rev. Lett.* **122** 218501